# Small-Signal Stability for Parallel-Connected Inverters in Stand-Alone AC Supply Systems

Ernane Antônio Alves Coelho, Porfírio Cabaleiro Cortizo, and Pedro Francisco Donoso Garcia, *Member, IEEE*

***Abstract*—This paper presents a small-signal analysis for parallel-connected inverters in stand-alone ac supply systems. The control technique of the inverters is based on frequency and voltage droops, which depends on the local variable measurements and does not need control interconnections. Simulation and experimental results show that the system is well represented by the small-signal model. Some root locus plots for the system are provided, which make the stability studies and design easier.**

***Index Terms*—Frequency and voltage droops, parallel connection, small-signal stability, voltage inverters.**

## I. Introduction

NOWADAYS, the proliferation of critical loads (e.g., satellite systems, air traffic control systems, Internet nodes, bank transactions, and life support equipment) implies the necessity of high-reliability uninterruptible power supply (UPS) systems. The UPS system reliability can be improved substantially by parallel connection of two or more units, as can be seen in [2], [3], and [12].

Several approaches to connect converters in parallel are proposed in [4], [8], [14], [15], [18], and [23]. All these schemes require control interconnections to provide load sharing. In order to increase the system reliability by addition of redundancy, it is necessary to minimize the control communications, the master–slave relationship between the units connected in parallel must be avoided, and all units must be identical [22]. These requirements can be satisfied by the control scheme for parallel-connected inverters based on frequency and voltage droops, which is derived from electric power system control [3], [5]–[7], [9], [11], [12], [19]. The important characteristic of this kind of controller is that it uses only those variables that can be measured locally at the inverter, avoiding communication between control units of each inverter. This implies that whole stand-alone system composed of several units connected in parallel presents high reliability.

This paper provides a small-signal model for parallel-connected inverters to aid designers to choose the slope of droop characteristics as a function of the desired dynamic behavior of the system. Dynamic stability of electric power systems has been the subject of several studies for many years. Reference [21] shows how to perform the small-signal analysis for an arbitrary number of interconnected synchronous machines, using the techniques of modern control theory, where the system is described by a set of differential equations in state space of the form

$$[\dot{X}] = [A'][X] + [B'][U]. \tag{1}$$

In this case, the system input vector $[U]$ is a function of the state variables $[X]$ (see Section IV), resulting in the homogeneous equation (2), which describes the free motion of the system

$$[\dot{X}] = [A][X]. \tag{2}$$

Reference [21] presents a method of building up the $[A]$ matrix of the multimachine power system from the submatrices describing individual elements of the synchronous system. Using a similar method, this paper shows how to build the $[A]$ matrix of the system composed by an arbitrary number of parallel-connected inverters using a control strategy based on frequency and voltage droops.

## II. Control Scheme

A stand-alone power system fed by parallel synchronous machines presents inherent operating characteristics as follows.

1) Fast frequency variation or speed derivatives are limited by rotor inertia.
2) There is a natural coupling between the operating frequency and active output power, that is, to constant mechanical input power, the operating frequency decreases when the output power increases.
3) Two or more synchronous machines connected in parallel tend to remain in synchronism due to the synchronizing torque component.
4) The system stability depends on the existence of sufficient synchronizing torque and damping torque components.
5) Voltage stability is dependent on the demand for reactive power [13].

On the other hand, the power inverters do not present this natural connection between frequency and active output power, neither between output voltage and reactive output power. Therefore, in order to reach stable operation, when the inverters are connected in parallel, these inherent operating conditions must be established by the inverter's control system. Fig. 1 shows the control scheme of each inverter connected in a stand-alone system. Each inverter presents a classical pulsewdith modulation (PWM) controller with an inner current loop and an outer

Paper IPCSD 01–084, presented at the 2000 Industry Applications Society Annual Meeting, Rome, Italy, October 8–12, and approved for publication in the IEEE TRANSACTIONS ON INDUSTRY APPLICATIONS by the Industrial Power Converter Committee of the IEEE Industry Applications Society. Manuscript submitted for review May 1, 2000 and released for publication November 21, 2001.

E. A. A. Coelho is with the School of Electrical Engineering, Federal University of Uberlândia, 38400-902 Uberlândia, Brazil (e-mail: ernane@ufu.br).

P. C. Cortizo and P. F. D. Garcia are with the Electrical Engineering Research and Development Center, Federal University of Minas Gerais, 31270-901 Belo Horizonte, Brazil (e-mail: porfirio@cpdee.ufmg.br).

Publisher Item Identifier S 0093-9994(02)02672-5.

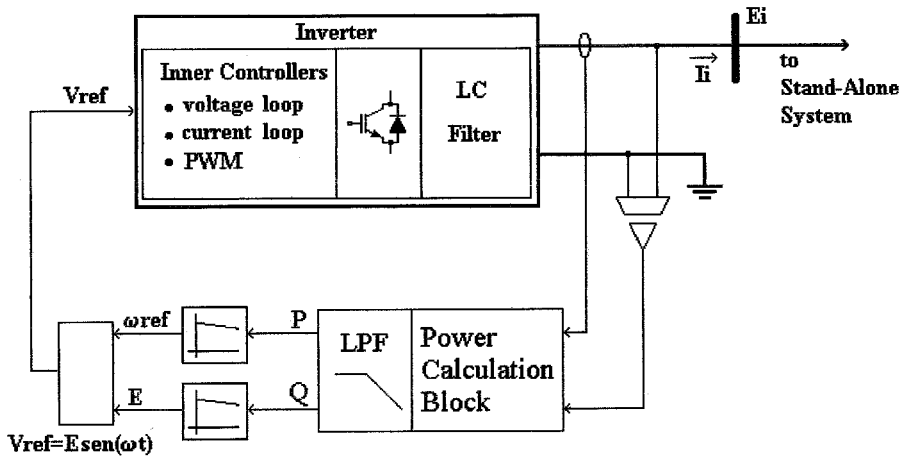


Fig. 1. Single-phase inverter connected to stand-alone system.

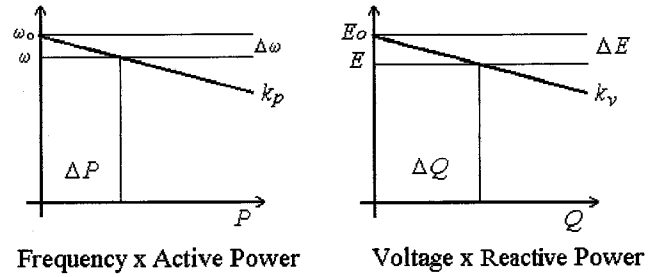


Fig. 2. Frequency and voltage droop.

voltage loop, both using proportional plus integral (PI) compensators. The sinusoidal reference for the outer voltage loop of each inverter is obtained in the reference block from the amplitude signal and frequency signal defined by power droop characteristics. Active power and reactive power are obtained in the power calculation block using a computational algorithm. Different from those specific schemes presented in [10] and [20], this one does not provide suitable current sharing under nonlinear loads. With the limited resources available in the laboratory, this work has concentrated on single-phase inverters, but the results can be easily extended to three-phase inverters with the additional advantages of the instantaneous power theory [1].

## III. Small-Signal Analysis of Each Inverter

Inverter output frequency $\omega$ and inverter output voltage $E$ are controlled by the droop characteristics defined by (3) and (4), respectively, which are represented in Fig. 2

$$\omega = \omega_o - k_p P \tag{3}$$

$$E = E_o - k_v Q. \tag{4}$$

In order to ensure the control laws defined by (3) and (4), it is necessary to measure the output power of each inverter. This measuring block uses a low-pass filter which makes the bandwidth of the power flux controller much smaller than the one of the voltage control loop of the inverter; then, the performance of the control will suffer a hard influence of this filter. In addition, the bandwidth of the inverter voltage control can be increased using several techniques, as can be seen in [16] and [17]. The inner controllers of the inverter have to provide active damping for possible oscillations between the output filters of the inverters and the transmission line, as can be seen in [3]. Therefore, we can consider the inverter an ideal voltage source with controllable amplitude and frequency. Then, the active and reactive output power obtained by the measuring block is given by (5) and (6), where $\omega_f$ is the cutoff frequency of the measuring filter and $s$ is the Laplace operator

$$P_{\text{meas}}(s) = \frac{\omega_f}{s+\omega_f} P(s) \tag{5}$$

$$Q_{\text{meas}}(s) = \frac{\omega_f}{s+\omega_f} Q(s). \tag{6}$$

According to [6], the linearized control equations of the system are

$$\Delta\omega(s) = -\frac{k_p\omega_f}{s+\omega_f} \Delta P(s) \tag{7}$$

$$\Delta E(s) = -\frac{k_v\omega_f}{s+\omega_f} \Delta Q(s). \tag{8}$$

Thus, considering (7) and (8) in the time domain,

$$\Delta\dot{\omega} = -\omega_f\Delta\omega - k_p\omega_f\Delta P \tag{9}$$

$$\Delta\dot{E} = -\omega_f\Delta E - k_v\omega_f\Delta Q \tag{10}$$

where $\Delta$ denotes the small deviation of the respective variable from the equilibrium point and a dotted variable represents the derivative with respect to time.

Considering a common $d$–$q$ reference frame for all inverters, we can represent the vector $\vec{E}$ as

$$\vec{E} = e_d + je_q \tag{11}$$

where

$$e_d = E\cos(\delta) \tag{12}$$

$$e_q = E\sin(\delta) \tag{13}$$

$$\delta = \arctan\left(\frac{e_q}{e_d}\right). \tag{14}$$

Linearizing the equation for $\delta$, which is the angular position of the vector $\vec{E}$, we have

$$\Delta\delta = \frac{\partial\delta}{\partial e_d}\Delta e_d + \frac{\partial\delta}{\partial e_q}\Delta e_q \tag{15}$$

then, it follows that

$$\Delta\delta = m_d\Delta e_d + m_q\Delta e_q \tag{16}$$

where

$$m_d = -\frac{e_q}{e_d^2+e_q^2} \tag{17}$$

$$m_q = \frac{e_d}{e_d^2+e_q^2}. \tag{18}$$

Since

$$\Delta\omega(s) = s\Delta\delta(s) \tag{19}$$

it implies that

$$\Delta\omega = m_d\Delta\dot{e_d} + m_q\Delta\dot{e_q}. \tag{20}$$

Considering that

$$E = |\vec{E}| = \sqrt{e_d^2+e_q^2} \tag{21}$$

we can linearize (21), thus,

$$\Delta E = n_d\Delta e_d + n_q\Delta e_q \tag{22}$$

where

$$n_d = \frac{e_d}{\sqrt{e_d^2+e_q^2}} \tag{23}$$

$$n_q = \frac{e_q}{\sqrt{e_d^2+e_q^2}}. \tag{24}$$

It follows that

$$\Delta\dot{E} = n_d\Delta\dot{e_d} + n_q\Delta\dot{e_q}. \tag{25}$$

Solving the equation system formed by expressions (10), (20), (22), and (25) for variables $\Delta\dot{e_d}$ and $\Delta\dot{e_q}$, we have

$$\Delta\dot{e_d} = \frac{n_q}{m_dn_q - m_qn_d}\Delta\omega + \frac{m_qn_d\omega_f}{m_dn_q - m_qn_d}\Delta e_d + \frac{m_qn_q\omega_f}{m_dn_q - m_qn_d}\Delta e_q + \frac{k_vm_q\omega_f}{m_dn_q - m_qn_d}\Delta Q \tag{26}$$

$$\Delta\dot{e_q} = \frac{n_d}{m_qn_d - m_dn_q}\Delta\omega + \frac{m_dn_d\omega_f}{m_qn_d - m_dn_q}\Delta e_d + \frac{m_dn_q\omega_f}{m_qn_d - m_dn_q}\Delta e_q + \frac{k_vm_d\omega_f}{m_qn_d - m_dn_q}\Delta Q. \tag{27}$$

Considering (9), (26), and (27), we can obtain the state equation (28), which describes the behavior of each inverter

$$\begin{bmatrix}\Delta\dot{\omega_i}\\ \Delta\dot{e_{di}}\\ \Delta\dot{e_{qi}}\end{bmatrix} = [M_i]\begin{bmatrix}\Delta\omega_i\\ \Delta e_{di}\\ \Delta e_{qi}\end{bmatrix} + [C_i]\begin{bmatrix}\Delta P_i\\ \Delta Q_i\end{bmatrix}. \tag{28}$$

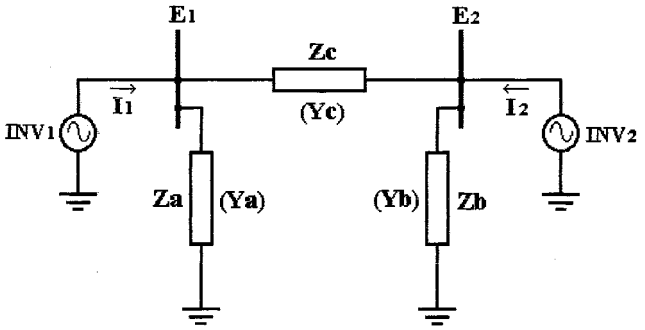


Fig. 3. Stand-alone system with two inverters.

## IV. Small-Signal Analysis for the Whole System

In order to make this analysis easier, we consider a system composed of two inverters connected to a network, as shown in Fig. 3, but it can be extended for an arbitrary number of inverters.

Since the variation in the network frequency is considered very small, the network is assumed to be completely described by the nodal admittance matrix equation

$$\begin{bmatrix}\vec{I_1}\\ \vec{I_2}\end{bmatrix} = \begin{bmatrix}Y_a+Y_c & -Y_c\\ -Y_c & Y_b+Y_c\end{bmatrix}\begin{bmatrix}\vec{E_1}\\ \vec{E_2}\end{bmatrix}. \tag{29}$$

We can transform the complex equation (29) in its real form

$$\begin{bmatrix}i_{d1}\\ i_{q1}\\ i_{d2}\\ i_{q2}\end{bmatrix} = \begin{bmatrix}G_{11} & -B_{11} & G_{12} & -B_{12}\\ B_{11} & G_{11} & B_{12} & G_{12}\\ G_{21} & -B_{21} & G_{22} & -B_{22}\\ B_{21} & G_{21} & B_{22} & G_{22}\end{bmatrix}\begin{bmatrix}e_{d1}\\ e_{q1}\\ e_{d2}\\ e_{q2}\end{bmatrix}. \tag{30}$$

Equation (30) can be written symbolically as

$$[i] = [Y_s][e]. \tag{31}$$

Linearizing the algebraic expression (31), we have

$$[\Delta i] = [Y_s][\Delta e]. \tag{32}$$

Considering the expressions for active and reactive power supplied by each inverter,

$$P_i = e_{di}i_{di} + e_{qi}i_{qi} \tag{33}$$

$$Q_i = e_{di}i_{qi} - e_{qi}i_{di}. \tag{34}$$

It implies that

$$\begin{bmatrix}\Delta P_1\\ \Delta Q_1\\ \Delta P_2\\ \Delta Q_2\end{bmatrix} = \begin{bmatrix}i_{d1} & i_{q1} & 0 & 0\\ i_{q1} & -i_{d1} & 0 & 0\\ 0 & 0 & i_{d2} & i_{q2}\\ 0 & 0 & i_{q2} & -i_{d2}\end{bmatrix}\begin{bmatrix}\Delta e_{d1}\\ \Delta e_{q1}\\ \Delta e_{d2}\\ \Delta e_{q2}\end{bmatrix} + \begin{bmatrix}e_{d1} & e_{q1} & 0 & 0\\ -e_{q1} & e_{d1} & 0 & 0\\ 0 & 0 & e_{d2} & e_{q2}\\ 0 & 0 & -e_{q2} & e_{d2}\end{bmatrix}\begin{bmatrix}\Delta i_{d1}\\ \Delta i_{q1}\\ \Delta i_{d2}\\ \Delta i_{q2}\end{bmatrix} \tag{35}$$

which in symbolic form is

$$[\Delta S] = [I_s][\Delta e] + [E_s][\Delta i]. \tag{36}$$

TABLE I
SYSTEM PARAMETERS AND EQUILIBRIUM POINT

| Variable | Value | Unit |
|---|---|---|
| Line transmission $(Z_c)$ | $0.5+j3$ | Ω |
| Local load - inverter 1 $(Z_a)$ | $13+j6$ | Ω |
| Local load - inverter 2 $(Z_b)$ | $25+j13$ | Ω |
| Cut-off frequency of measuring filter $(\omega_f)$ | 37.7 | rd/s |
| Frequency droop coefficient $(k_p)$ | 0.0005 | rd/s/W |
| Voltage droop coefficient $(k_v)$ | 0.0005 | V/VAR |
| Inverter output apparent power 1 $(P_1+jQ_1)$ | $806+j384$ | VA |
| Inverter output apparent power 2 $(P_2+jQ_2)$ | $750+j375$ | VA |
| Inverter output voltage 1 $(\vec{E_1})$ | $127+j0$ | V (rms) |
| Inverter output voltage 2 $(\vec{E_2})$ | $129.9+j4.7$ | V (rms) |
| Inverter output current 1 $(\vec{I_1})$ | $6.4-j3$ | A (rms) |
| Inverter output current 2 $(\vec{I_2})$ | $5.9-j2.7$ | A (rms) |
| Nominal frequency at operating point | 377 | rd/s |

Substituting (32) in (36), we obtain

$$[\Delta S] = ([I_s] + [E_s][Y_s])\,[\Delta e]. \tag{37}$$

The state equation for the whole system can be written as [see (28)]

$$\begin{bmatrix} \Delta\dot{\omega}_1 \\ \Delta\dot{e}_{d1} \\ \Delta\dot{e}_{q1} \\ \Delta\dot{\omega}_2 \\ \Delta\dot{e}_{d2} \\ \Delta\dot{e}_{q2} \end{bmatrix} = \begin{bmatrix} M_1 & 0 \\ 0 & M_2 \end{bmatrix} \begin{bmatrix} \Delta\omega_1 \\ \Delta e_{d1} \\ \Delta e_{q1} \\ \Delta\omega_2 \\ \Delta e_{d2} \\ \Delta e_{q2} \end{bmatrix} + \begin{bmatrix} C_1 & 0 \\ 0 & C_2 \end{bmatrix} \begin{bmatrix} \Delta P_1 \\ \Delta Q_1 \\ \Delta P_2 \\ \Delta Q_2 \end{bmatrix} \tag{38}$$

which is written symbolically as

$$[\Delta\dot{X}] = [M_s][\Delta X] + [C_s][\Delta S]. \tag{39}$$

Combining (39) and (37), we have

$$[\Delta\dot{X}] = [M_s][\Delta X] + [C_s]\,([I_s] + [E_s][Y_s])\,[\Delta e]. \tag{40}$$

Considering that

$$\begin{bmatrix} \Delta e_{d1} \\ \Delta e_{q1} \\ \Delta e_{d2} \\ \Delta e_{q2} \end{bmatrix} = \begin{bmatrix} 0 & 1 & 0 & 0 & 0 & 0 \\ 0 & 0 & 1 & 0 & 0 & 0 \\ 0 & 0 & 0 & 0 & 1 & 0 \\ 0 & 0 & 0 & 0 & 0 & 1 \end{bmatrix} \begin{bmatrix} \Delta\omega_1 \\ \Delta e_{d1} \\ \Delta e_{q1} \\ \Delta\omega_2 \\ \Delta e_{d2} \\ \Delta e_{q2} \end{bmatrix} \tag{41}$$

or symbolically

$$[\Delta e] = [K_s][\Delta X]. \tag{42}$$

Substituting (42) in (40), we have

$$[\Delta\dot{X}] = [A][\Delta X] \tag{43}$$

where

$$[A] = [M_s] + [C_s]\,([I_s] + [E_s][Y_s])\,[K_s]. \tag{44}$$

Equation (43) describes the free motion of the system for small disturbances around the equilibrium point, that is, the behavior of the $\Delta\omega_1$, $\Delta e_{d1}$, $\Delta e_{q1}$, $\Delta\omega_2$, $\Delta e_{d2}$, and $\Delta e_{q2}$ around an operating point defined by $\omega_1$, $e_{d1}$, $e_{q1}$, $\omega_2$, $e_{d2}$, and $e_{q2}$ from a given small initial condition. The power flow analysis must be done to calculate the operating point.

## V. SIMULATION RESULTS

Some simulations were made in order to validate the present small-signal analysis. Two examples for different frequency and voltage droop coefficients are presented in simulation studies.

### A. Example I

These simulation results were obtained considering the system shown in Fig. 3 with the parameters presented in Table I. The offset of frequency droop and voltage droop was tuned so that each inverter provides the power specified in Table I at 377 rd/s.

Considering that the initial active and reactive output powers are zero, and that initial vectors $\vec{E_1}$ and $\vec{E_2}$ are in phase, we can build the matrix $[A]$ of the system, and obtain the respective eigenvalues, which are

$$\begin{aligned} \lambda_1 &= \;\;0.0 \\ \lambda_2 &= -6.4 \\ \lambda_3 &= -31.4 \\ \lambda_4 &= -35.4 \\ \lambda_5 &= -37.6 \\ \lambda_6 &= -37.7. \end{aligned}$$

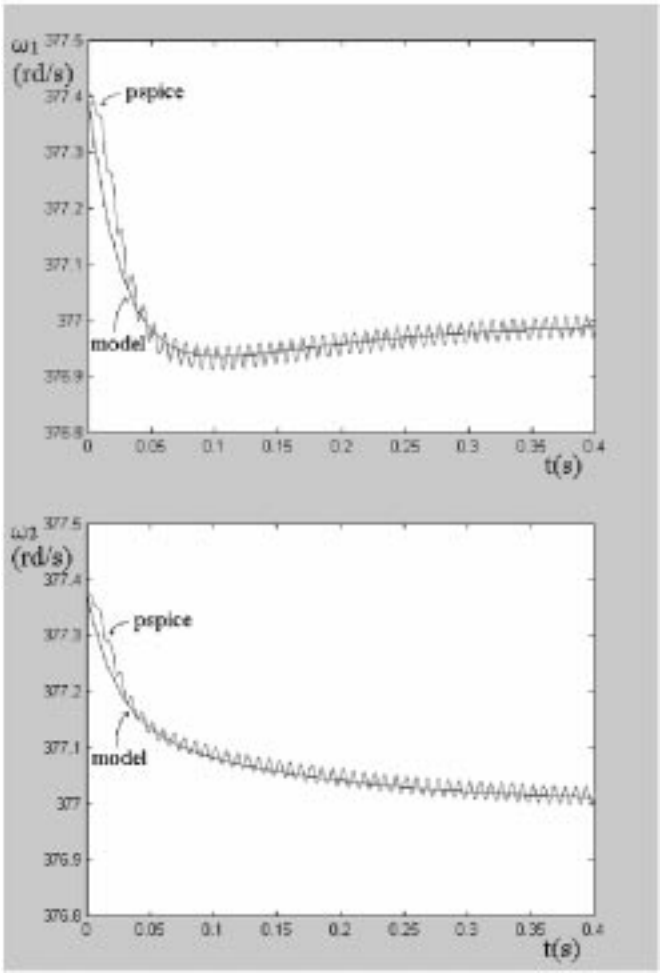


Fig. 4. Frequency waveform of inverters 1 and 2.

According to [3], the set of angles $\Delta\delta_i$ is linearly dependent, and matrix $[A]$ is singular and has a zero eigenvalue. Only the nonzero eigenvalues of $A$ are important for the stability studies. Then, the system presents five negative real eigenvalues and, consequently, it has a stable damped response. Fig. 4 presents the frequency waveform of each inverter obtained by (43) and the simulation of the system in Pspice, which corresponds to the numerical solution of the nonlinear system equations. We can observe that the system is well represented by the small-signal model. It is important to keep in mind that (43) provides the deviations from the equilibrium point, and that the behavior of variables is determined by the following equation:

$$[X] = [X]_{\text{eq.point}} + [\Delta X(0)]e^{[A]t}. \tag{45}$$

The active and reactive powers are presented in Fig. 5. The oscillations at 120 Hz are not completely eliminated by the measuring filter from the power measurements. The reactive power flux is faster than the active power flux and both present a damped response.

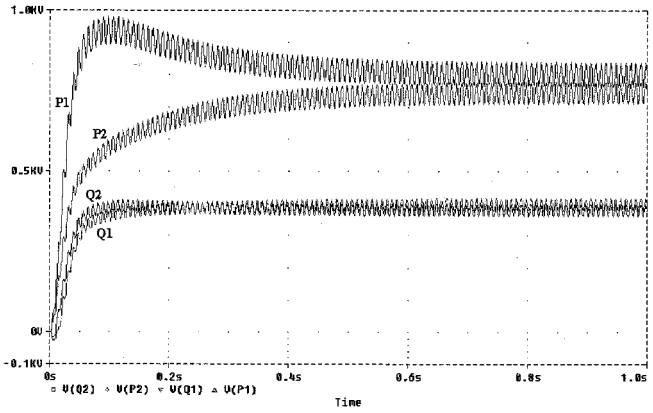


Fig. 5. Active and reactive power.

### B. Example II

Using the same procedure for Example I, but increasing $k_p$ and $k_v$ ten times, we can build the matrix $[A]$ again, obtaining the following eigenvalues:

$$\begin{aligned}
\lambda_1 &= \ \ 0.0 \\
\lambda_2 &= -19.3 + j40.8 \\
\lambda_3 &= -19.3 - j40.8 \\
\lambda_4 &= -19.9 \\
\lambda_5 &= -36.6 \\
\lambda_6 &= -37.7.
\end{aligned}$$

Now, the system presents eigenvalues with a nonzero imaginary part, therefore, with an oscillatory response. The negative real part of eigenvalues implies that oscillations are damped. Fig. 6 presents the frequency waveform of the inverters by the small-signal model and simulation in Pspice. The results are very close one more time.

The active and reactive powers are presented in Fig. 7. The power flux in this case is faster than in Example I, but it is underdamped.

## VI. Experimental Results

Two PWM inverters were assembled in order to validate theoretical studies. The scheme for each inverter is shown in Fig. 8. It consists of a single-phase insulated gate bipolar transistor (IGBT) inverter connected to a stand-alone ac system, as seen in Fig. 3. The inverter presents a classical PI control with inner current loop and outer voltage loop. The dc bus was obtained by a three-phase rectifier, which implies that only positive active power flux is possible. The part of the scheme shown in the shaded area consists of the power flux control, which uses a 133-MHz PC computer and an acquisition system (PC30DS). Besides the power flux control function, the control software presents two other functions. First, we have a phased-locked-loop (PLL) block used to synchronize the inverter with the stand-alone system. Second, we have a control loop used to eliminate the average current presented in the system due to a small offset in the inverter output voltage.

First of all, inverter 1 is connected to the system supplying all the load. The IGBT gate drivers of inverter 2 are disabled,

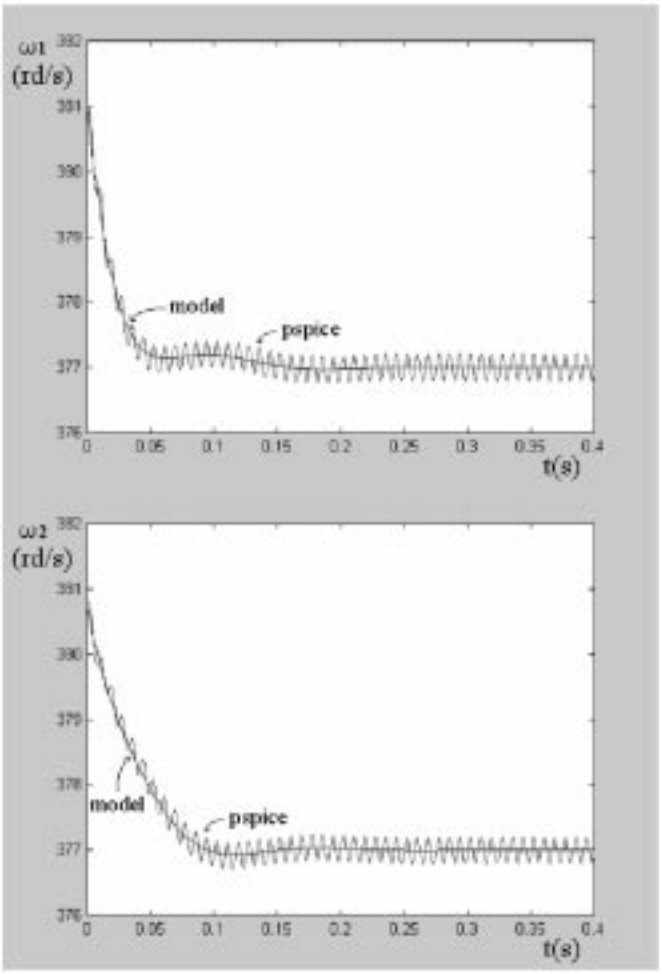


Fig. 6. Frequency waveform of inverters 1 and 2.

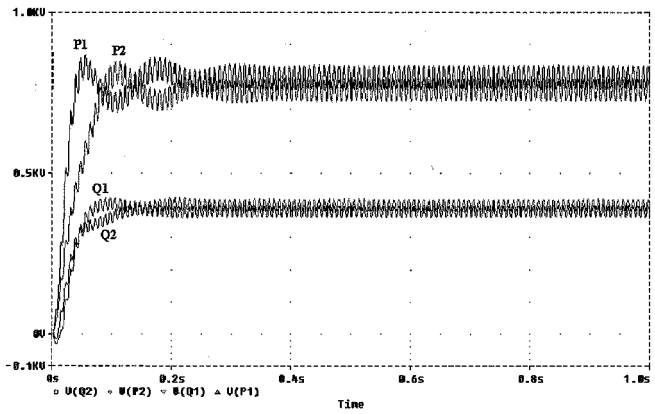


Fig. 7. Active and reactive power.

and then the switch *SW1* is closed. An ac voltage appears in the filter capacitor of inverter 2 due to the stand-alone system. Therefore, the reference voltage of inverter 2 is synchronized with the capacitor voltage by the PLL block. When reference voltage and output voltage are in phase, *SW2* (software switch) is changed from state 1 to state 2, and the IGBT gate drivers are simultaneously enabled through a parallel port.

Two tests for different frequency and voltage droops were done and the respective results are presented next. In each test, the frequency droop and voltage droop offsets were tuned in a way that the inverters share the load as specified in Table II. Inverter frequency waveforms are presented and compared with the frequency defined by the small-signal model.

The acquisition system presents a digital second-order filter with cutoff frequency at 1 kHz in order to eliminate the inverter switching noise. The samples are transferred to computer using direct memory access (DMA) techniques. Both the acquisition system and digital power control loop run at 5 kHz.

### A. Test I

The parameters used in Test I are presented in Table II. The values have no particular reason, being defined as a function of the resources available in the laboratory. Fig. 9 presents the experimental inverter frequency and the inverter frequency defined by the small-signal model. The power flux control, the control loop for average output current, and the IGBT gate drivers were enabled 0.1 s after the acquisition system started to save data. It can be seen that the real system is well represented by the model. Before the power control and the IGBT gate drivers are enabled, the behavior of the frequency of inverter 2 is defined by the dynamic response of the PLL block.

Fig. 10 shows the active and reactive powers provided by both inverters. Before the power flux control is enabled, inverter 1 supplies all the load and the active output power for inverter 2 is zero. We can observe that, after inverter 2 is connected to the system, the load active power is conveniently shared by the inverters.

The filter capacitor of inverter 2 provides a reactive power for the stand-alone system, then, the reactive power for inverter 2 does not start from zero. It can be seen that the reactive powers do not converge exactly to the set point specified in Table II, but it is important to take into account that an error of 1.0 V in inverter output voltage implies a deviation of 2000 var in reactive power setpoint, considering a voltage droop of 0.0005 V/var.

The output voltage and output current for each inverter are shown in Fig. 11. The current scale is enlarged ten times. Observing the amplitude and phase of the output current and output voltage of each inverter, we can verify its correspondence with the power fluxes obtained.

### B. Test II

The parameters used in Test II are the same as those presented in Table II, except that $k_p$ and $k_v$ for both inverters were increased ten times, that is, $k_p = 0.005$ W/rd/s and $k_v = 0.005$ V/var. Fig. 12 presents the experimental inverter frequency and the inverter frequency defined by the small-signal model. The power flux control, the control loop for average output current, and the IGBT gate drivers were enabled 0.05 s after the acquisition system started to save data. Now, the system is faster than the performance presented in Test I and presents an underdamped oscillatory response.

Fig. 13 shows the active and reactive power for the inverters. The sharing of power flux is performed faster than in Test I.

The output voltage and output current for each inverter are shown in Fig. 14. The current scale is ten times higher than the normal scale. As can be seen in Test I, the current and voltage waveforms correspond to the power fluxes obtained. Before it

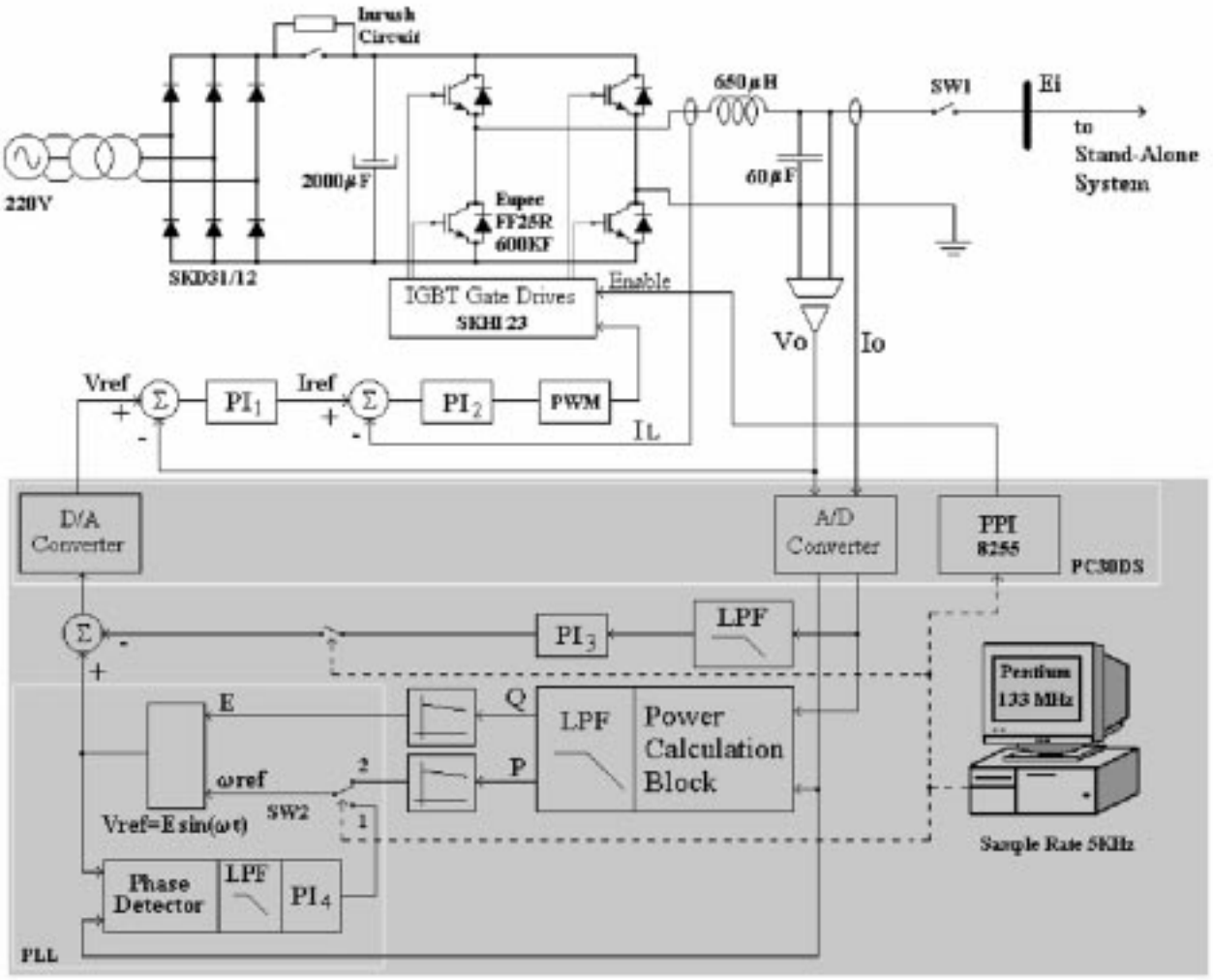


Fig. 8. Scheme for each inverter.

TABLE II
SYSTEM PARAMETERS AND EQUILIBRIUM POINT

| Variable | Value | Unit |
|---|---|---|
| Line transmission $(Z_c)$ | $0.2+j3.1$ | Ω |
| Local load - inverter 1 $(Z_a)$ | $25.7+j27.2$ | Ω |
| Local load - inverter 2 $(Z_b)$ | $52+j9$ | Ω |
| Cut-off frequency of measuring filter $(\omega_f)$ | 37.7 | rd/s |
| Frequency droop coefficient $(k_p)$ | 0.0005 | rd/s/W |
| Voltage droop coefficient $(k_v)$ | 0.0005 | V/VAR |
| Inverter output apparent power 1 $(P_1+jQ_1)$ | $298+j187$ | VA |
| Inverter output apparent power 2 $(P_2+jQ_2)$ | $280+j180$ | VA |
| Inverter output voltage 1 $(\vec{E}_1)$ | $127+j0$ | V (rms) |
| Inverter output voltage 2 $(\vec{E}_2)$ | $130.3-j1.2$ | V (rms) |
| Inverter output current 1 $(\vec{I}_1)$ | $2.3-j1.5$ | A (rms) |
| Inverter output current 2 $(\vec{I}_2)$ | $2.1-j1.4$ | A (rms) |
| Nominal frequency at operating point | 377 | rd/s |

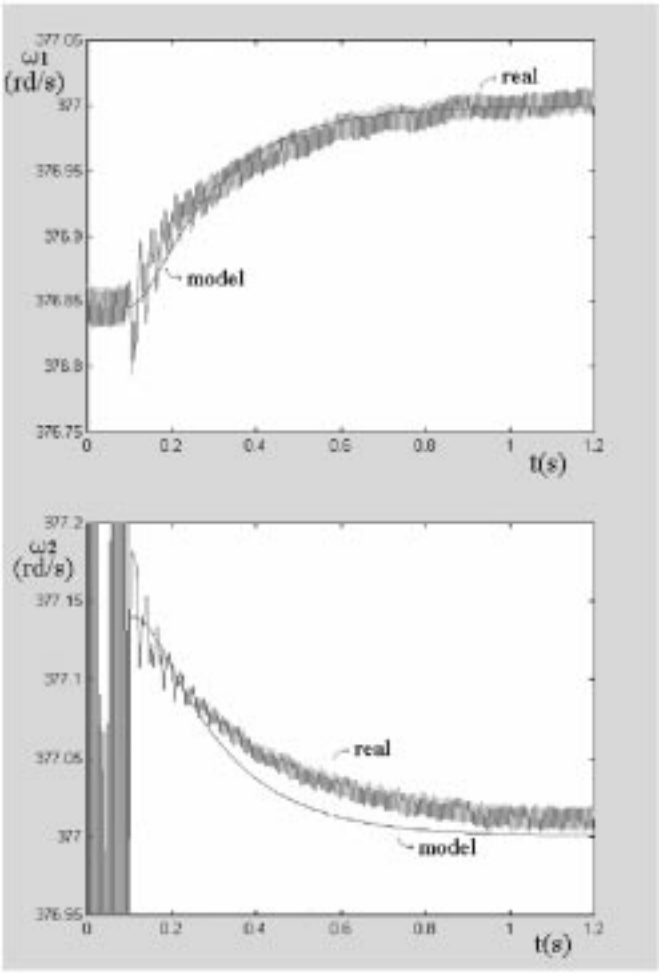


Fig. 9. Test I—real and model inverter frequency.

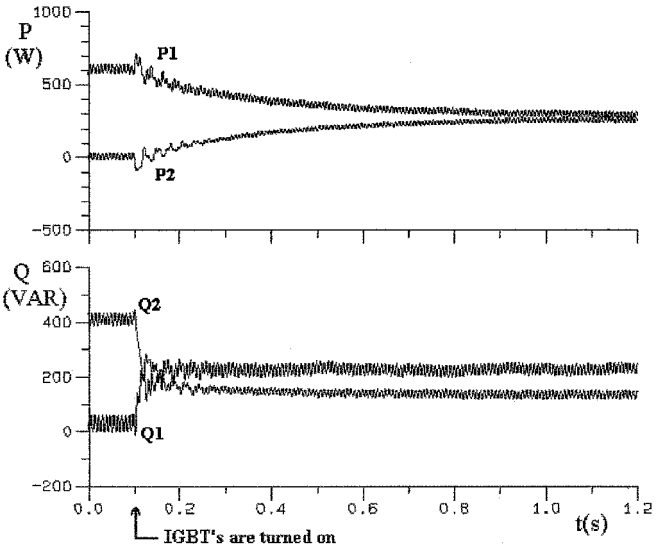


Fig. 10. Test I—active and reactive power for both inverters.

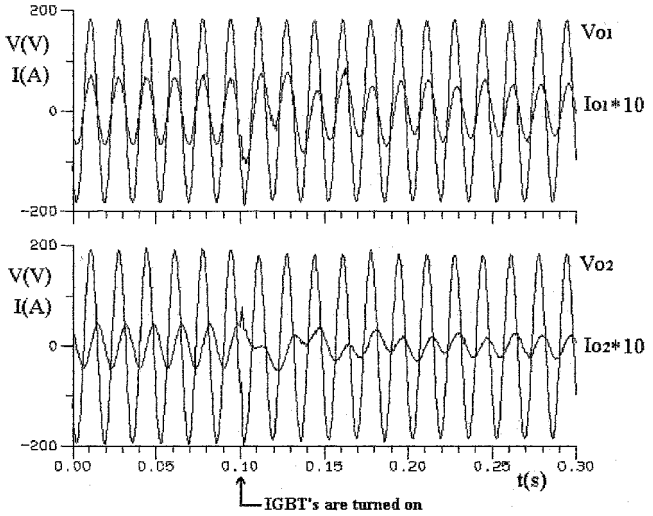


Fig. 11. Test I—output voltage and output current for both inverters.

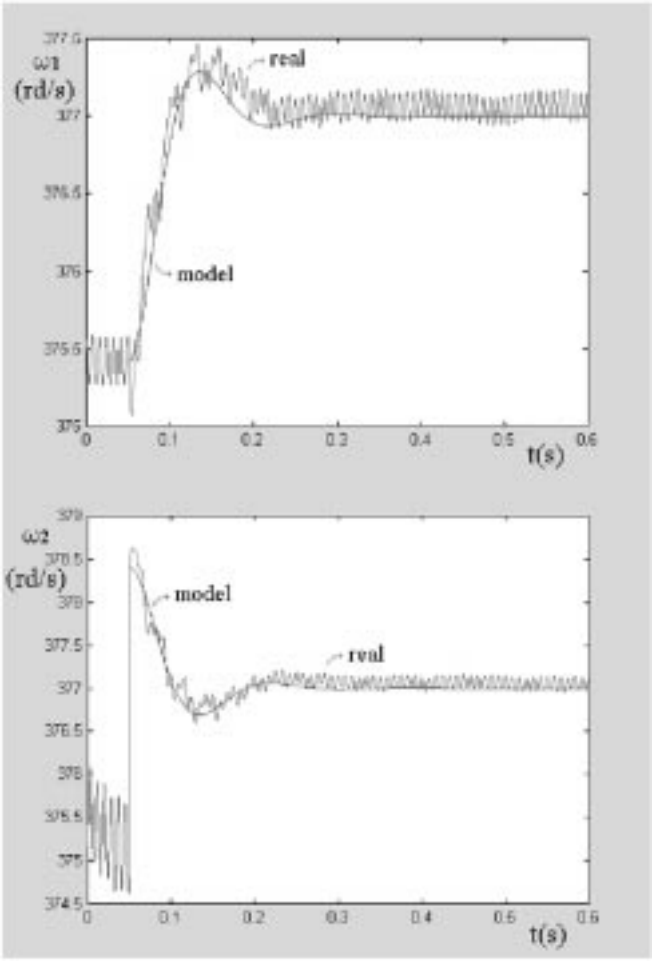


Fig. 12. Test II—real and model inverter frequency.

## VII. Dynamic Behavior of the System

In order to understand the dynamic behavior of the system, some root locus plots are shown as a function of given system parameters. Fig. 15 shows the root locus plot for the system (see

is connected to the system, the output current in inverter 2 is due to the current in the filter capacitor, that is, the current from inverter 2 lags by 90° the system voltage.

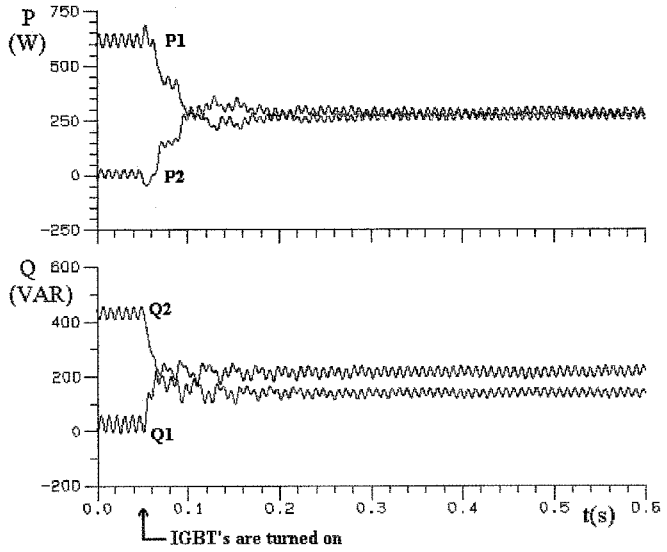


Fig. 13. Test II—active and reactive power for both inverters.

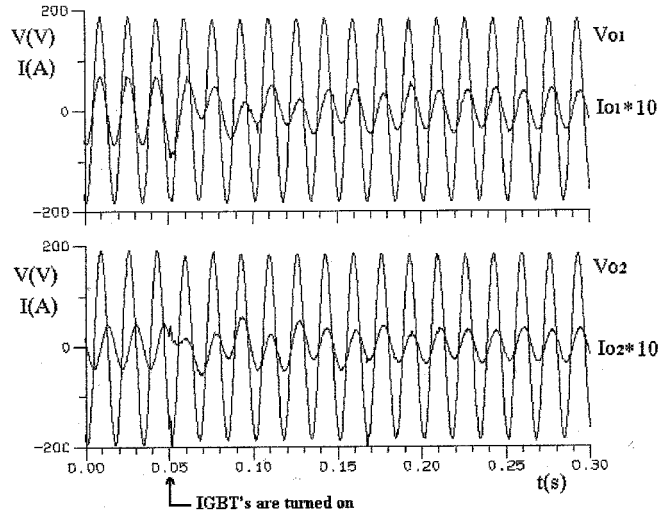


Fig. 14. Test II—output voltage and output current for both inverters.

Fig. 3 and Table II) considering a variation of the coefficients $k_p$ and $k_v$ from 0.0001 to 0.01 rd/s/W (V/var). Note that the system has an underdamped response for higher values of the parameters $k_p$ and $k_v$. The critical damping occurs for $k_p = k_v = 0.001$ rd/s/W (V/var). The pole at origin ($\lambda_1$) does not move and the system remains stable over the entire range. It is important to take into account that higher values of $k_p$ imply larger frequency changes and the small-signal model does not represent the system very well.

Fig. 16 shows the root locus plot for the system as a function of the variation of the inductance of the transmission line from 0.1 to 10 mH, considering $k_p = k_v = 0.005$ rd/s/W (V/var). It can be seen that the system becomes unstable for lower values of the transmission line inductance. It is important to bear in mind that a minimal impedance to connect inverters in parallel is necessary. It is possible to find in electrical power system generators bussed together at their terminals, but, in this case, the load compensation control uses the internal impedance and regulates the voltage within the generator to provide the load sharing [13]. Internal states instead of output voltage must be controlled to provide load sharing for inverters connected in parallel at their terminals. The control scheme shown in Fig. 8 is not suitable for this approach.

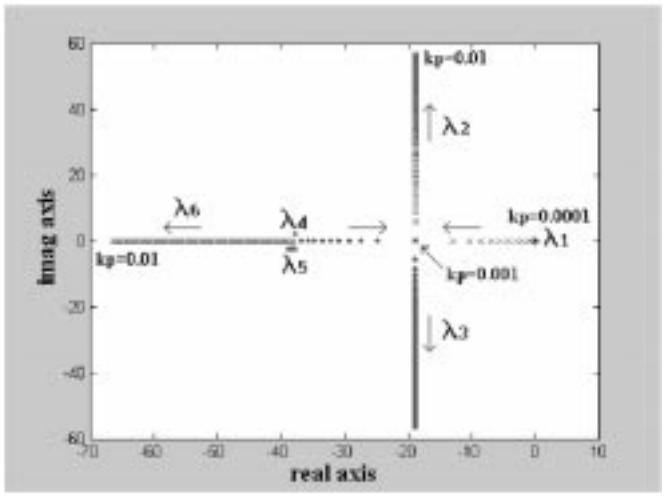


Fig. 15. Root locus plot $0.0001 < k_p = k_v < 0.01$.

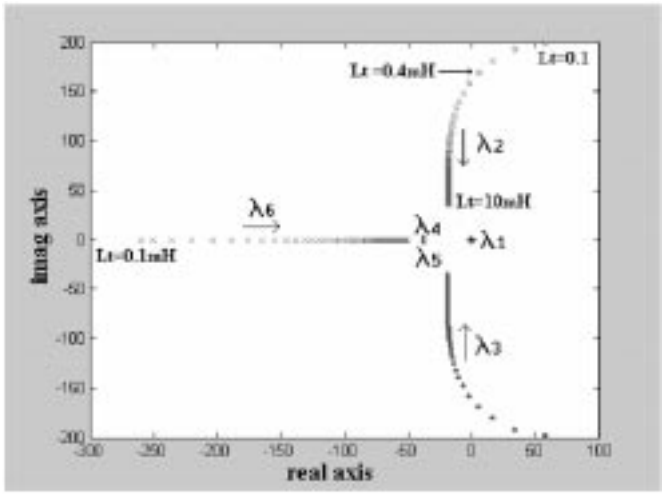


Fig. 16. Root locus plot $0.1 < L_t < 10$ mH.

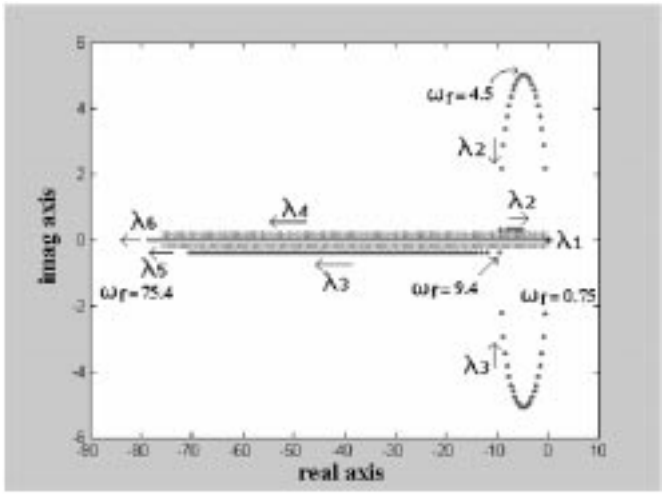


Fig. 17. Root locus plot $0.75 < \omega_f < 75.4$ rd/s.

Fig. 17 shows the root locus plot for the system as a function of the measuring filter cutoff frequency ($\omega_f$) over the range from

0.75 to 75.4 rd/s. The system response becomes underdamped for lower values of cutoff frequency. The higher the cutoff frequency, the faster the system response, since the power signal ripple does not cause the system instability, because this fact is not considered by the model.

## VIII. Conclusion

This paper has presented a small signal analysis for parallel connected inverters in stand-alone AC supply systems, which makes stability and performance studies easier. Simulation and experimental results show that the system is well represented by the proposed small signal model.

Based on the model, several root locus plots as a function of the system parameters can be obtained in order to help designers to define optimal values of $k_p$, $k_v$, transmission line inductance and measuring filter cutoff frequency for an improved performance of the system.

## References


[1] H. Akagi, Y. Kanazawa, and A. Nabae, "Generalized theory of the instantaneous reactive power in three-phase circuits," in *Proc. IPEC*, 1983, pp. 1375–1386.

[2] M. C. Chandorkar, D. M. Divan, Y. Hu, and B. Banerjee, "Novel architectures and control for distributed ups systems," in *Proc. IEEE APEC'94*, 1994, pp. 683–689.

[3] M. C. Chandorkar, "Distributed uninterruptible power supply systems," Ph.D. dissertation, WEMPEC, Univ. Wisconsin, Madison, WI, 1995.

[4] J.-F. Chen and C.-L. Chu, "Combination voltage-controlled and current controlled PWM inverters for ups parallel operation," *IEEE Trans. Power Electron.*, vol. 10, pp. 547–558, Sept. 1995.

[5] E. A. A. Coelho, "Técnicas de controle aplicadas ao paralelismo de inversores," Ph.D. dissertation, Dept. Elect. Eng., Federal Univ. Minas Gerais, Belo Horizonte, Brazil, 2000.

[6] E. A. A. Coelho, P. C. Cortizo, and P. F. D. Garcia, "Small signal stability for single phase inverter connected to stiff ac system," in *Conf. Rec. IEEE-IAS Annu. Meeting*, vol. 4, Oct. 1999, pp. 2180–2187.

[7] ——, "Small signal stability for parallel connected inverters in stand-alone ac supply systems," in *Conf. Rec. IEEE-IAS Annu. Meeting*, Oct. 2000, pp. 2345–2352.

[8] E. A. A. Coelho, P. C. Cortizo, P. F. D. Garcia, and B. R. Meneses, "Sliding mode controller for parallel connected inverters," in *Proc. IEEE CIEP'98*, Oct. 1998, pp. 96–102.

[9] D. M. Divan, M. C. Chandorkar, and R. Adapa, "Control of parallel connected inverter in stand-alone ac supply systems," in *Conf. Rec. IEEE-IAS Annu. Meeting*, 1991, pp. 1003–1009.

[10] U. B. Jensen, F. Blaabjerg, and P. N. Enjeti, "Sharing of nonlinear loads in parallel connected three-phase converters," in *Conf. Rec. IEEE-IAS Annu. Meeting*, vol. 5, Oct. 2000, pp. 2338–2345.

[11] T. Kawabata, S. Doi, T. Morikawa, T. Nakamura, and M. Shigenobu, "Large capacity parallel redundant transistor ups," in *Proc. IEEJ IPEC*, Mar. 1983, vol. 1, pp. 660–671.

[12] T. Kawabata and S. Higashino, "Parallel operation of voltage source inverters," *IEEE Trans. Ind. Applicat.*, vol. 24, pp. 281–287, Mar./Apr. 1988.

[13] P. S. Kundur, *Power System Stability and Control*. New York: McGraw-Hill, 1994.

[14] C. Q. Lee, K. Siri, and T. F. Wu, "Dynamic current distribution controls of a parallel connected converter system," in *Proc. IEEE PESC'91*, 1991, pp. 875–881.

[15] C. S. Lee, S. Kim, C. B. Kim, S. C. Hong, J. S. Yoo, S. W. Kim, C. H. Kim, S. H. Woo, and S. Y. Sun, "Parallel u.s.p. with a instantaneous current sharing control," in *Proc. IEEE IECON'98*, 1998, pp. 568–573.

[16] M. J. Ryan, W. E. Brumsickle, and R. D. Lorenz, "Control topology options for single-phase ups inverters," *IEEE Trans. Ind. Applicat.*, vol. 33, pp. 493–500, Mar./Apr. 1997.

[17] M. J. Ryan and R. D. Lorenz, "A high performance sine wave inverter controller with capacitor current feedback and 'back-emf' decoupling," in *Proc. IEEE PESC'95*, Atlanta, GA, 1995, pp. 507–513.

[18] K. Siri and C. Q. Lee, "Current distribution control of converters connected in parallel," in *Conf. Rec. IEEE-IAS Annu. Meeting*, Oct. 1990, pp. 1274–1280.

[19] A. Tuladhar, H. Jin, T. Unger, and K. Mauch, "Parallel operation of single phase inverter modules with no control interconnections," in *Proc. IEEE APEC'97*, vol. 1, Atlanta, GA, Feb. 1997, pp. 94–100.

[20] ——, "Control of parallel inverters in distributed ac power systems with consideration of line impedance effect," in *Proc. IEEE APEC'98*, 1998, pp. 321–328.

[21] J. M. Undrill, "Dynamic stability calculations for an arbitrary number of interconnected synchronous machines," *IEEE Trans. Power App. Syst.*, vol. PAS–87, pp. 835–844, Mar. 1968.

[22] A. van der Krans and K. Bouwknegt, "A control strategy for the redundant parallel operation of an ensemble of static ups systems of the parallel type," in *Proc. EPE Firenze*, 1991, pp. 148–152.

[23] T. F. Wu, Y. H. Huang, Y. K. Chen, and Z. R. Liu, "A 3c strategy for multi-module inverters in parallel operation to achieve an equal current distribution," in *Proc. IEEE PESC'98*, 1998, pp. 186–192.


**Ernane Antônio Alves Coelho** was born in Teófilo Otoni, Brazil, in 1962. He received the B.S. degree in electrical engineering from the Federal University of Minas Gerais, Belo Horizonte, Brazil, the M.S. degree from the Federal University of Santa Catarina, Florianópolis, Brazil, and the Ph.D. degree from the Federal University of Minas Gerais in 1987, 1989, and 2000, respectively.

He is currently with the Power Electronics Research Group, Federal University of Uberlândia, Uberlândia, Brazil. His research interests are PWM inverters, power-factor correction, and digital control by microcontrollers and DSPs.

**Porfírio Cabaleiro Cortizo** was born in Belo Horizonte, Brazil, in 1955. He received the B.S. degree in electrical engineering from the Federal University of Minas Gerais, Belo Horizonte, Brazil, and the Dr.Ing. degree from the Institut Polytechnique de Toulouse, Toulouse, France, in 1978 and 1984, respectively.

Since 1978, he has been with the Electronic Engineering Department, Federal University of Minas Gerais, where he is currently a Professor of Electrical Engineering. His research interests include high-frequency and high-efficiency switching power converter UPS systems, power active filters, and control systems.

**Pedro Francisco Donoso Garcia** (S'88–M'92) received the B.S. degree in electronic engineering from the Universidade Federal do Rio Grande do Sul, Porto Alegre, Brazil, the M.S. degree in electrical and electronics engineering from the Universidade Federal de Minas Gerais, Belo Horizonte, Brazil, and the Ph.D. degree in electrical and electronics engineering from the Universidade Federal de Santa Catarina, Florianópolis, Brazil, in 1981, 1986, and 1991, respectively.

He is currently an Associate Professor in the Department of Electronic Engineering, Universidade Federal de Minas Gerais. His research interests include high-frequency and high-efficiency switching power converter UPS systems, power active filters, and audio amplifiers.